J. Opt. A: Pure Appl. Opt. **11** (2009) 114011 (11pp) doi:10.1088/1464-4258/11/11/114011

Theoretical and experimental investigation of radiative decay rates in active slot waveguides

C Creatore[1,2], L C Andreani[2], M Galli[2], M Miritello[3], R Lo Savio[3] and F Priolo[3]

[1] Dipartimento di Fisica, Politecnico di Torino, Corso duca degli Abruzzi 24, I-10129 Torino, Italy
[2] Dipartimento di Fisica 'A Volta', Università degli Studi di Pavia, via Bassi 6, I-27100 Pavia, Italy
[3] MATIS CNR-INFM and Dipartimento di Fisica e Astronomia, Università di Catania, Via S Sofia 64, I-95123 Catania, Italy

E-mail: creatore@fisicavolta.unipv.it

Received 30 January 2009, accepted for publication 21 April 2009
Published 16 September 2009
Online at stacks.iop.org/JOptA/11/114011

Abstract
We present a quantum-electrodynamical formalism to study the spontaneous emission from dipoles embedded in a non-absorbing and lossless multilayer dielectric structure. In this model the electromagnetic field is quantized by a proper choice of a complete and orthonormal set of classical modes and the analytical expressions for the emission rates are obtained within the framework of perturbation theory. We apply our model to investigate the 1.54 μm transition of Er^{3+}-doped SiO_2 thin layers acting as active material in planar slot waveguides in polycrystalline silicon. The theoretical results show that a strong reduction of the radiative lifetime does occur in the slot waveguide. Furthermore, by using the theoretical analysis together with photoluminescence measurements, we estimate also the radiative efficiency which is found to be only slightly reduced with respect to the value for Er^{3+} in a bulk of SiO_2. These results are important for future realization of silicon-compatible active optical devices and show the relevance of our model to study the spontaneous emission processes in multilayer structures.

Keywords: active silicon waveguides, theory of spontaneous emission, theory and experiments

(Some figures in this article are in colour only in the electronic version)

1. Introduction

Since the pioneering work by Purcell [1] it is well known that the modifications in the electromagnetic (e.m.) boundary conditions induced by the material surrounding an excited atom can considerably affect its rate of spontaneous emission (SE). Such an effect can be explained either within classical electromagnetism, in terms of a self-driven dipole due to the reflected field at the dipole position, or in the framework of quantum electrodynamics, as emission stimulated by zero-point fluctuations of the e.m. field, both descriptions yielding the same results as long as the coupling between the atom and the field is weak. In such a *weak coupling* regime, the SE rate can be derived within first-order perturbation theory by applying Fermi's Golden Rule, and is proportional to the local coupling of the atomic dipole moment to the allowed photon modes, i.e. to the local density of states (LDoS) [2]: when the LDoS vanishes, then the SE process is inhibited while, whereas an increase in the density of states occurs, the rate of SE can be enhanced over the free space value.

Extensive literature is available dealing with the analysis of SE from various emitters (such as atoms, molecules or electron–hole pairs) embedded in dielectric environments of varying complexity. In a homogeneous medium with dielectric constant ε, Glauber has shown [3] that the SE rate relative to the free space value is enhanced (reduced) when $\varepsilon > 1$ (<1). One of the most studied configurations is the single dielectric interface [4–11] as it is the simplest model system where

experimental and theoretical analysis can be performed in order to get the basic understanding necessary to investigate more complex structures. In more complicated systems both the technology and the theory needed are more demanding, but the expected effects turn out also to be more interesting. For instance, among multiple dielectric layers structures, planar microcavities have been intensively studied during the last few years [12–15], due to their ability to considerably affect the density of states and thus to strongly modify the emission into a particular mode, which is of crucial importance for the development of novel light-emitting devices.

In this work we study the spontaneous emission process in a generic non-dispersive and lossless multilayer dielectric structure and derive the SE rates by applying a fully quantum-electrodynamical formalism. Our aim is twofold: (i) to develop a model suitable for different configurations, thus taking into account all the possible modes (and the related SE rates) which can be excited in the examined structure and (ii) to get a quantitative insight into the modifications of the atomic radiative processes which occur in realistic structures such as active silicon-based optical waveguides. Such structures, which nowadays can be tailored according to different geometries—from simple waveguides to multilayer-like configurations—are characterized by an high-index contrast and are able to confine and guide light very efficiently in nanometer-size spatial regions as a result of total internal reflection. These waveguiding and confining properties, together with the low propagation losses typical of silicon and the good compatibility with complementary metal oxide semiconductor technology, make them very appealing for the future development of highly integrated multifunctional optoelectronic and photonic devices (see, e.g., [16–18] and the review works by Kenyon [19] and Polman [20]). Recently, slot configurations have been proposed to improve the waveguiding/confining properties of silicon-based optical waveguides [21, 22]. In this novel structure a very thin (a few tens of nanometers thick) layer (slot) of low-index material is bounded by two high-index material regions (typically silicon) which form the core of an optical waveguide. The high-index contrast interfaces at the slot are able to concentrate the e.m. field in very narrow spatial regions ($\ll\lambda$), thus leading to an enhancement of the radiation–matter interaction. Also, due to the increase of vacuum e.m. field fluctuations, an enhancement in the spontaneous emission rate is expected to occur, similarly to what happens with the well-known Purcell effect [1] for an emitter in an optical cavity. A theoretical study [23] of the emission properties of a planar slot waveguide doped with erbium ions, as well as the experimental evidence [24] of the enhanced light–matter coupling, have already been reported. Here we present a detailed study of the modifications induced in the 1.54 μm transition of Er^{3+}-doped SiO_2 layers acting as the active material in deposited polycrystalline silicon slot waveguides. A combined analysis based on time-resolved PL measurements and our model is consistent with a strong increase of the radiative decay rate in the slot waveguide, when compared with values obtained investigating three other configurations. Furthermore, we estimate that the radiative efficiency is marginally reduced with respect to the value of Er^{3+} in a bulk of SiO_2, so that radiative recombination is still the dominant decay mechanism in these active slot waveguides.

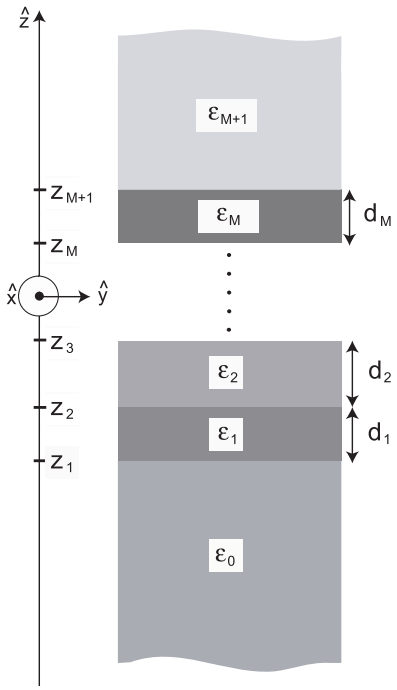

Figure 1. Schematic view of the multilayer dielectric structure. The semi-infinite lower (0) and the upper ($M+1$) cladding layers with dielectric constants ε_0 and ε_{M+1}, respectively, surround a stack of M dielectric layers, each one being d_j thick and characterized by an average dielectric constant ε_j, $j = 1, \ldots, M$.

This paper is organized as follows. In section 2 the modes supported by the multilayer dielectric structure (leaky and guided modes) are listed and described. In particular we show that, when dealing with radiation emission problems, a basis for leaky modes characterized by a single outgoing component is more suitable than the standard one generally used. In section 3, by using a second-quantized form for the atom–field interaction Hamiltonian and perturbation theory, we derive the analytical expressions for the SE rates as a function of the dipole position. In section 4 we show the theoretical and experimental analysis of the 1.54 μm transition of Er^{3+}-doped SiO_2 layers acting as active material in deposited polycrystalline silicon slot waveguides and in three other configurations, namely after deposition on SiO_2 and crystalline Si (c-Si) substrates and embedded in an oxide bulk. A short summary of the results is given in section 5.

2. Model system and field modes

We are interested in the evaluation of the SE rate from a dipole embedded in a system like the one depicted in figure 1, i.e. a stack of M dielectric layers which are parallel to the xy plane and assumed to be infinite along the x and y directions. Each layer has a thickness of d_j ($j = 1, \ldots, M$) and the lower and upper cladding layers (layers 0 and $M+1$, respectively, in figure 1) are semi-infinite. All the $M+2$ layers are assumed to be lossless, isotropic and homogeneous along the vertical

(z) direction. The overall dielectric constant $\varepsilon(\mathbf{r}) = \varepsilon(\boldsymbol{\rho}, z)$ is thus a piecewise constant function in the z direction, i.e. we use $\varepsilon_j = \varepsilon_j(z)$, $j = 0, \ldots, M+1$. Hence, since the whole system is homogeneous in the xy plane the field modes will be factorized as $\mathbf{E}(\mathbf{r}, t)[\mathbf{H}(\mathbf{r}, t)] = \mathrm{e}^{-\mathrm{i}\omega t + \mathrm{i}\mathbf{k}_\parallel \cdot \boldsymbol{\rho}}\mathbf{E}(z)[\mathbf{H}(z)]$, where $\mathbf{k}_\parallel = k_\parallel \hat{k}_\parallel = (k_x, k_y)$ is the in-plane propagation vector. The classical modes supported by such a structure and needed to set up a quantum theory for the spontaneous emission are the solutions of the following eigenvalue problem:

$$\nabla \times \left[\frac{1}{\varepsilon(\mathbf{r})}\nabla \times \mathbf{H}\right] = \frac{\omega^2}{c^2}\mathbf{H}, \tag{1}$$

which results from the homogeneous Maxwell equations for the electric and magnetic fields $\mathbf{E}$, $\mathbf{H}$ with harmonic time dependence $\exp(-\mathrm{i}\omega t)$, and the condition $\nabla \cdot \mathbf{H} = 0$ being fulfilled. The modes form a complete and orthonormal set, i.e.

$$\mathbf{H}(\mathbf{r}) = \sum_\mu c_\mu \mathbf{H}_\mu(\mathbf{r}), \tag{2}$$

$$\int \mathbf{H}^*_\mu(\mathbf{r}) \cdot \mathbf{H}_\nu(\mathbf{r}) \mathrm{d}\mathbf{r} = \delta_{\mu\nu}. \tag{3}$$

The electric field eigenmodes, which can be obtained from $\mathbf{E}(\mathbf{r}) = \{[ic]/[\omega\varepsilon(\mathbf{r})]\}\nabla \times \mathbf{H}(\mathbf{r})$, are also orthonormal [25]:

$$\int \varepsilon(\mathbf{r})\mathbf{E}^*_\mu(\mathbf{r}) \cdot \mathbf{E}_\nu(\mathbf{r})\, \mathrm{d}\mathbf{r} = \delta_{\mu\nu}. \tag{4}$$

In a lossless multilayer dielectric structure, the complete and orthonormal set of classical modes consists of an infinite number of leaky modes and a finite number of guided (or trapped) modes. Leaky modes can be either fully or partially leaky. The former modes, similar to free space modes, radiate in both the lower and upper cladding, while the latter ones radiate only in the cladding with the higher refractive index and propagate out of the smaller index cladding layer as evanescent waves with exponentially decreasing amplitude. Guided modes are in-plane traveling modes, trapped (confined) by the highest refractive index layer (if there is any) and characterized by an evanescent field profile across the z direction.

While guided modes are uniquely specified by the Maxwell equations with the proper continuity conditions across the dielectric boundaries, leaky modes are not, since their asymptotic behavior ($z \to \pm\infty$) has to be characterized, such a characterization being not unique.

Usually the basis of leaky modes is described in terms of the triplets incident–reflected–transmitted waves, with waves incoming towards the multilayer stack either from the lower or from the upper cladding layer (see figure 2(a)). This set of modes, also known as Carniglia and Mandel modes (as they originally introduced such a classification [25]), has been widely employed to specify the leaky states in structures like dielectric waveguides [26, 27] or planar dielectric microcavities [13, 28]. Such a choice, however, is not the most convenient when dealing with radiation emission analysis. As shown in figure 2(a), both the reflected and the transmitted components (the pairs $\{\mathrm{r}_l, \mathrm{t}_u\}$ or $\{\mathrm{r}_u, \mathrm{t}_l\}$), which belong to two different modes, contribute to the total emission in a given direction. Hence, quantum interference between

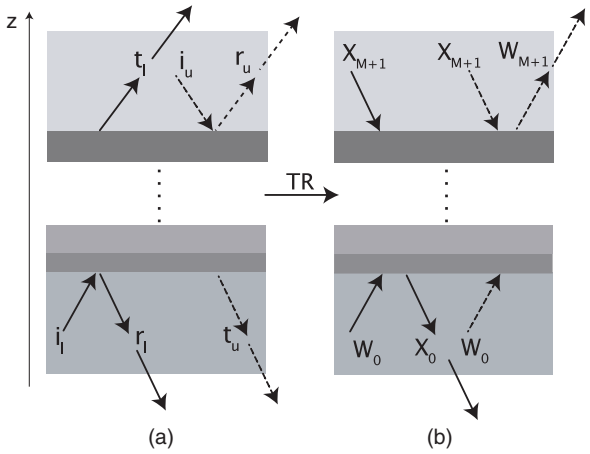

Figure 2. The leaky modes in a multilayer dielectric structure. (a) The standard set of modes based on the triplets incident–reflected–transmitted waves; $\{\mathrm{i}_l, \mathrm{r}_l, \mathrm{t}_l\}$ for waves incoming from the lower cladding, $\{\mathrm{i}_u, \mathrm{r}_u, \mathrm{t}_u\}$ for waves incoming from the upper cladding. (b) The set of modes specified by a single outgoing component and two incoming waves (towards the stack): $\{X_0, W_0, X_{M+1}\}$ for states outgoing in the lower cladding, $\{W_{M+1}, W_0, X_{M+1}\}$ for states outgoing in the upper cladding. The notation is valid for TE-polarized modes; for TM polarization one replaces $W \to Y$ and $X \to Z$.

these two different outgoing modes has to be explicitly taken into account in the definition of the local density of leaky states [29, 30] and the calculation of the emission in either the upper or the lower cladding layer turns out to be problematic. To avoid this subtle interference problem and calculate in a simple way the fraction of emission in either the upper or the lower cladding layer or, in general, the SE patterns, we use a set of leaky modes specified by a single outgoing wave. Within this basis, the single outgoing component comes together with two incoming waves propagating towards the structure, as shown in figure 2(b) with the triplets $\{W_{M+1}, W_0, X_{M+1}\}$ and $\{X_0, W_0, X_{M+1}\}$ for states outgoing in the upper and lower cladding layers, respectively. The total emission signal is thus completely specified by one outgoing mode only—either by the component labeled as W_{M+1} for leaky modes outgoing in the upper cladding or by the component X_0 for states outgoing in the lower cladding—and interference terms never arise. It is worth noticing that this set of modes can be obtained from the Carniglia and Mandel modes previously discussed (which is specified in terms of the incoming waves) after application of a time-reversal (TR) operator [23]. Since the algebraic properties are invariant under time-reversal operations, this new set is also orthonormal and complete. In the following a detailed description of both guided and leaky field profiles is given.

2.1. Leaky modes

As previously discussed, the basis of leaky modes used in our model is defined by a single outgoing component and two ingoing ones. In each of the M layers the field is a superposition of two counter-propagating modes. The modes are defined by their propagation wavevector $\mathbf{k} = (\mathbf{k}_\parallel, q)$, with

the z component q in each of the $M+2$ media being

$$q_j = \sqrt{\varepsilon_j \frac{\omega^2}{c^2} - k_\parallel^2}, \qquad j = 0, \ldots, M+1. \tag{5}$$

With $\hat{\varepsilon}_{\mathbf{k}_\parallel} = \hat{z} \times \hat{k}_\parallel$ we denote the unit vector orthogonal to both $\mathbf{k}_\parallel = k_\parallel \hat{k}_\parallel$ and $\hat{z}$ and set $z_1 = -d_1/2$, $z_j = z_{j-1} + d_{j-1}$ with $j = 2, \ldots, M+1$. For TE polarization the field profiles are

$$\mathbf{E}^{\mathrm{TE}}_{\mathbf{k}_\parallel}(\boldsymbol{\rho}, z) = \frac{\mathrm{e}^{\mathrm{i}\mathbf{k}_\parallel \cdot \boldsymbol{\rho}}}{\sqrt{V}} \mathrm{i}\hat{\varepsilon}_{\mathbf{k}_\parallel} E^{\mathrm{TE}}(k_\parallel, z), \tag{6}$$

$$\mathbf{H}^{\mathrm{TE}}_{\mathbf{k}_\parallel}(\boldsymbol{\rho}, z) = \frac{\mathrm{e}^{\mathrm{i}\mathbf{k}_\parallel \cdot \boldsymbol{\rho}}}{\sqrt{V}} \mathrm{i}\frac{c}{\omega} [H^{\mathrm{TE}}_\perp(k_\parallel, z)\hat{z} + H^{\mathrm{TE}}_\parallel(k_\parallel, z)\hat{k}_\parallel], \tag{7}$$

where V is a normalization box volume which disappears in the final expressions and the time dependence $\mathrm{e}^{-\mathrm{i}\omega t}$ is implicit. The expressions for the amplitudes E^{TE}, $H^{\mathrm{TE}}_\perp$ and $H^{\mathrm{TE}}_\parallel$ are as follows:

$$E^{\mathrm{TE}}(k_\parallel, z) = \begin{cases} W_{M+1}\mathrm{e}^{\mathrm{i}q_{M+1}(z-z_{M+1})} \\ \quad + X_{M+1}\mathrm{e}^{-\mathrm{i}q_{M+1}(z-z_{M+1})}, & z > z_{M+1} \\ W_j \mathrm{e}^{\mathrm{i}q_j(z-z_j-d_j/2)} \\ \quad + X_j \mathrm{e}^{-\mathrm{i}q_j(z-z_j-d_j/2)}, \\ \qquad z_j < z < z_j + d_j \\ W_0 \mathrm{e}^{\mathrm{i}q_0(z-z_1)} + X_0 \mathrm{e}^{-\mathrm{i}q_0(z-z_1)}, & z < z_1 \end{cases} \tag{8}$$

$$H^{\mathrm{TE}}_\perp(k_\parallel, z) = \begin{cases} k_\parallel[W_{M+1}\mathrm{e}^{\mathrm{i}q_{M+1}(z-z_{M+1})} \\ \quad + X_{M+1}\mathrm{e}^{-\mathrm{i}q_{M+1}(z-z_{M+1})}], & z > z_{M+1} \\ k_\parallel[W_j \mathrm{e}^{\mathrm{i}q_j(z-z_j-d_j/2)} \\ \quad + X_j \mathrm{e}^{-\mathrm{i}q_j(z-z_j-d_j/2)}], \\ \qquad z_j < z < z_j + d_j \\ k_\parallel[W_0 \mathrm{e}^{\mathrm{i}q_0(z-z_1)} \\ \quad + X_0 \mathrm{e}^{-\mathrm{i}q_0(z-z_1)}], & z < z_1 \end{cases} \tag{9}$$

$$H^{\mathrm{TE}}_\parallel(k_\parallel, z) = \begin{cases} q_{M+1}[X_{M+1}\mathrm{e}^{-\mathrm{i}q_{M+1}(z-z_{M+1})} \\ \quad - W_{M+1}\mathrm{e}^{\mathrm{i}q_{M+1}(z-z_{M+1})}], & z > z_{M+1} \\ q_j[X_j \mathrm{e}^{-\mathrm{i}q_j(z-z_j-d_j/2)} \\ \quad - W_j \mathrm{e}^{\mathrm{i}q_j(z-z_j-d_j/2)}], \\ \qquad z_j < z < z_j + d_j \\ q_0[X_0 \mathrm{e}^{-\mathrm{i}q_0(z-z_1)} \\ \quad - W_0 \mathrm{e}^{\mathrm{i}q_0(z-z_1)}]. & z < z_1. \end{cases} \tag{10}$$

The amplitudes for leaky modes outgoing in the lower (upper) cladding (see figure 2(b)) are found taking $W_{M+1} = 0$ ($X_0 = 0$) in (8)–(10) and through the normalization condition (3) which yields $X_0 = 1/\sqrt{\varepsilon_0}$ ($W_{M+1} = 1/\sqrt{\varepsilon_{M+1}}$); all the other amplitudes are then obtained by applying a standard transfer-matrix theory. It is worth noticing that the normalization condition for leaky modes (leading to the values given above for the amplitudes X_0 and W_{M+1}) is determined by the cladding regions only: when $L \gg d$, L being the width of the normalization box in the z direction and d the thickness of the waveguide core (or the thickness of a stack of layers for a generic multilayer structure), the contributions from the core (stack) are of the order $\mathrm{O}(d/L)$ and thus negligibly small if compared to the contributions from the semi-infinite cladding regions.

When the dielectric constants of the upper and lower claddings are different and the conditions for total internal reflection are matched, the modes become partially leaky. Without loss of generality, we now assume $\varepsilon_0 > \varepsilon_{M+1}$. In this case, when $\omega(\sqrt{\varepsilon_{M+1}}/c) \leqslant k_\parallel \leqslant \omega(\sqrt{\varepsilon_0}/c)$, the emission occurs in the lower cladding layer only and the field is evanescent in the upper cladding, the z component q_{M+1} being purely imaginary. The field amplitudes can still be obtained through the same conditions given above for the fully leaky modes, but taking $W_{M+1} = 0$ and replacing q_{M+1} with its complex conjugate in (8)–(10).

The field profiles for TM-polarized modes are

$$\mathbf{H}^{\mathrm{TM}}_{\mathbf{k}_\parallel}(\boldsymbol{\rho}, z) = \frac{\mathrm{e}^{\mathrm{i}\mathbf{k}_\parallel \cdot \boldsymbol{\rho}}}{\sqrt{V}} \mathrm{i}\hat{\varepsilon}_{\mathbf{k}_\parallel} H^{\mathrm{TM}}(k_\parallel, z), \tag{11}$$

$$\mathbf{E}^{\mathrm{TM}}_{\mathbf{k}_\parallel}(\boldsymbol{\rho}, z) = \frac{\mathrm{e}^{\mathrm{i}\mathbf{k}_\parallel \cdot \boldsymbol{\rho}}}{\sqrt{V}} \mathrm{i}\frac{c}{\varepsilon_j \omega} [E^{\mathrm{TM}}_\perp(k_\parallel, z)\hat{z} + E^{\mathrm{TM}}_\parallel(k_\parallel, z)\hat{k}_\parallel], \tag{12}$$

with amplitudes given by

$$H^{\mathrm{TM}}(k_\parallel, z) = \begin{cases} Y_{M+1}\mathrm{e}^{\mathrm{i}q_{M+1}(z-z_{M+1})} \\ \quad + Z_{M+1}\mathrm{e}^{-\mathrm{i}q_{M+1}(z-z_{M+1})}, & z > z_{M+1} \\ Y_j \mathrm{e}^{\mathrm{i}q_j(z-z_j-d_j/2)} + Z_j \mathrm{e}^{-\mathrm{i}q_j(z-z_j-d_j/2)}, \\ \qquad z_j < z < z_j + d_j \\ Y_0 \mathrm{e}^{\mathrm{i}q_0(z-z_1)} + Z_0 \mathrm{e}^{-\mathrm{i}q_0(z-z_1)}, & z < z_1 \end{cases} \tag{13}$$

$$E^{\mathrm{TM}}_\perp(k_\parallel, z) = \begin{cases} k_\parallel[Y_{M+1}\mathrm{e}^{\mathrm{i}q_{M+1}(z-z_{M+1})} \\ \quad + Z_{M+1}\mathrm{e}^{-\mathrm{i}q_{M+1}(z-z_{M+1})}], \\ \qquad z > z_{M+1} \\ k_\parallel[Y_j \mathrm{e}^{\mathrm{i}q_j(z-z_j-d_j/2)} \\ \quad + Z_j \mathrm{e}^{-\mathrm{i}q_j(z-z_j-d_j/2)}], \\ \qquad z_j < z < z_j + d_j \\ k_\parallel[Y_0 \mathrm{e}^{\mathrm{i}q_0(z-z_1)} + Z_0 \mathrm{e}^{-\mathrm{i}q_0(z-z_1)}], \\ \qquad z < z_1 \end{cases} \tag{14}$$

$$E^{\mathrm{TM}}_\parallel(k_\parallel, z) = \begin{cases} q_{M+1}[Z_{M+1}\mathrm{e}^{-\mathrm{i}q_{M+1}(z-z_{M+1})} \\ \quad - Y_{M+1}\mathrm{e}^{\mathrm{i}q_{M+1}(z-z_{M+1})}], \\ \qquad z > z_{M+1} \\ q_j[Z_j \mathrm{e}^{-\mathrm{i}q_j(z-z_j-d_j/2)} \\ \quad - Y_j \mathrm{e}^{\mathrm{i}q_j(z-z_j-d_j/2)}], \\ \qquad z_j < z < z_j + d_j \\ q_0[Z_0 \mathrm{e}^{-\mathrm{i}q_0(z-z_1)} - Y_0 \mathrm{e}^{\mathrm{i}q_0(z-z_1)}]. \\ \qquad z < z_1. \end{cases} \tag{15}$$

In this case, fully leaky modes outgoing in the lower (upper) cladding have $Y_{M+1} = 0$ ($Z_0 = 0$) and the normalization condition (3) yields $Z_0 = 1$ ($Y_{M+1} = 1$) for the amplitude of the outgoing component. Similarly as done for TE-polarized modes, all the other coefficients are straightforwardly found after a standard transfer-matrix calculation. For modes which are partially radiating in the lower cladding (and evanescent in the upper cladding), one takes $Y_{M+1} = 0$ and replaces q_{M+1} with its complex conjugate in (13)–(15).

2.2. Guided modes

A multilayer dielectric structure like the one depicted in figure 1 is able to support a set of guided modes if the relation $\varepsilon_j = \varepsilon_{\max} > \varepsilon_0, \varepsilon_{M+1}$ holds for at least one of the inner layers ($j = 1, \ldots, M$) of the stack. Since guided modes are in-plane propagating modes, they will be labeled by a joint index $\mu = (\mathbf{k}_\parallel, \alpha)$, $\mathbf{k}_\parallel = k_\parallel \hat{k}_\parallel$ being the in-plane wavevector and α the mode index ($\geqslant 1$). Also, by $q_{j\mu}$ we denote the z component of the guided mode wavevector:

$$q_{j\mu} = \sqrt{\varepsilon_j(\omega_\mu^2/c^2) - k_\parallel^2}. \qquad j = 1, \ldots, M, \tag{16}$$

where $\omega_\mu = \omega_{\mathbf{k}_\parallel \alpha}$ is the frequency of the αth guided mode. In the upper ($j = M+1$) and lower ($j = 0$) cladding layers $q_{j\mu}$ becomes purely imaginary, $q_{j\mu} = \mathrm{i}\chi_{j\mu}$ with $\chi_{j\mu} = \sqrt{k_\parallel^2 - \varepsilon_j(\omega_\mu^2/c^2)}$, and thus the field $\propto \exp(\pm \mathrm{i} q_{j\mu} z)$ decays exponentially along the z direction. In the following we give their explicit form, obtained through a generalization of the standard theory for slab waveguides (see, e.g., [31, 32]).

For TE polarization the modes are given by

$$\mathbf{E}^{\mathrm{TE}}_{\mathbf{k}_\parallel}(\boldsymbol{\rho}, z) = \frac{\mathrm{e}^{\mathrm{i}\mathbf{k}_\parallel \cdot \boldsymbol{\rho}}}{\sqrt{S}} \mathrm{i} \frac{\omega_\mu}{c} \hat{\varepsilon}_{\mathbf{k}_\parallel} E^{\mathrm{TE}}(k_\parallel, z), \tag{17}$$

$$\mathbf{H}^{\mathrm{TE}}_{\mathbf{k}_\parallel}(\boldsymbol{\rho}, z) = \frac{\mathrm{e}^{\mathrm{i}\mathbf{k}_\parallel \cdot \boldsymbol{\rho}}}{\sqrt{S}} [H^{\mathrm{TE}}_\perp(k_\parallel, z)\hat{z} + H^{\mathrm{TE}}_\parallel(k_\parallel, z)\hat{k}_\parallel], \tag{18}$$

where S is a normalization surface which cancels in the final expressions and E^{TE}, $H^{\mathrm{TE}}_\perp$ and $H^{\mathrm{TE}}_\parallel$ are as follows. The field amplitudes for TE-polarized guided modes are

$$E^{\mathrm{TE}}(k_\parallel, z) = \begin{cases} A_{M+1\,\mu} \mathrm{e}^{-\chi_{M+1,\mu}(z - z_{M+1})}, \\ \qquad z > z_{M+1} \\ A_{j\mu} \mathrm{e}^{\mathrm{i}q_{j\mu}(z - z_j - d_j/2)} \\ + B_{j\mu} \mathrm{e}^{-\mathrm{i}q_{j\mu}(z - z_j - d_j/2)}, \\ \qquad z_j < z < z_j + d_j \\ B_{0\mu} \mathrm{e}^{\chi_{0\mu}(z - z_1)}, \qquad z < z_1 \end{cases} \tag{19}$$

$$H^{\mathrm{TE}}_\perp(k_\parallel, z) = \begin{cases} i A_{M+1\,\mu} k_\parallel \mathrm{e}^{-\chi_{M+1\,\mu}(z - z_{M+1})}, \\ \qquad z > z_{M+1} \\ i k_\parallel [A_{j\mu} \mathrm{e}^{\mathrm{i}q_{j\mu}(z - z_j - d_j/2)} \\ + B_{j\mu} \mathrm{e}^{-\mathrm{i}q_{j\mu}(z - z_j - d_j/2)}], \\ \qquad z_j < z < z_j + d_j \\ i B_{0\mu} k_\parallel \mathrm{e}^{\chi_{0\mu}(z - z_1)}, \qquad z < z_1 \end{cases} \tag{20}$$

$$H^{\mathrm{TE}}_\parallel(k_\parallel, z) = \begin{cases} A_{M+1\,\mu} \chi_{M+1\,\mu} \mathrm{e}^{-\chi_{M+1\,\mu}(z - z_{M+1})}, \\ \qquad z > z_{M+1} \\ i q_{j\mu} [B_{j\mu} \mathrm{e}^{-\mathrm{i}q_{j\mu}(z - z_j - d_j/2)} \\ - A_{j\mu} \mathrm{e}^{\mathrm{i}q_{j\mu}(z - z_j - d_j/2)}], \\ \qquad z_j < z < z_j + d_j \\ - B_{0\mu} \chi_{0\mu} \mathrm{e}^{\chi_{0\mu}(z - z_1)}, \qquad z < z_1 \end{cases} \tag{21}$$

where S is a normalization surface which cancels in the final expressions for the emission rates and the magnetic field is found by application of the Maxwell equation $\mathbf{H}(\mathbf{r}) = -\{(ic)/(\omega)\}\nabla \times \mathbf{E}(\mathbf{r})$. The $M+2$ coefficients in the expressions (19)–(21) are obtained through a standard transfer-matrix calculation together with the orthonormality condition (3) (see [23] for details)

TM-polarized guided modes are given by

$$\mathbf{H}^{\mathrm{TM}}_{\mathbf{k}_\parallel}(\boldsymbol{\rho}, z) = \frac{\mathrm{e}^{\mathrm{i}\mathbf{k}_\parallel \cdot \boldsymbol{\rho}}}{\sqrt{S}} \hat{\varepsilon}_{\mathbf{k}_\parallel} H^{\mathrm{TM}}(k_\parallel, z), \tag{22}$$

$$\mathbf{E}^{\mathrm{TM}}_{\mathbf{k}_\parallel}(\boldsymbol{\rho}, z) = \frac{\mathrm{e}^{\mathrm{i}\mathbf{k}_\parallel \cdot \boldsymbol{\rho}}}{\sqrt{S}} \frac{c}{\omega_\mu} [E^{\mathrm{TM}}_\perp(k_\parallel, z)\hat{z} + E^{\mathrm{TM}}_\parallel(k_\parallel, z)\hat{k}_\parallel], \tag{23}$$

with

$$H^{\mathrm{TM}}(k_\parallel, z) = \begin{cases} C_{M+1\,\mu} \mathrm{e}^{-\chi_{M+1,\mu}(z - z_{M+1})}, \\ \qquad z > z_{M+2} \\ C_{j\mu} \mathrm{e}^{\mathrm{i}q_{j\mu}(z - z_j - d_j/2)} \\ + D_{j\mu} \mathrm{e}^{-\mathrm{i}q_{j\mu}(z - z_j - d_j/2)}, \\ \qquad z_j < z < z_j + d_j \\ D_{0\mu} \mathrm{e}^{\chi_{0\mu}(z - z_1)}, \qquad z < z_1 \end{cases} \tag{24}$$

$$E^{\mathrm{TM}}_\perp(k_\parallel, z) = \begin{cases} (\mathrm{i}/\varepsilon_{M+1}) C_{M+1\,\mu} k_\parallel \mathrm{e}^{-\chi_{M+1\,\mu}(z - z_{M+1})}, \\ \qquad z > z_{M+1} \\ (\mathrm{i}/\varepsilon_j) k_\parallel [C_{j\mu} \mathrm{e}^{\mathrm{i}q_{j\mu}(z - z_j - d_j/2)} \\ + D_{j\mu} \mathrm{e}^{-\mathrm{i}q_{j\mu}(z - z_j - d_j/2)}], \\ \qquad z_j < z < z_j + d_j \\ (\mathrm{i}/\varepsilon_0) D_{0\mu} k_\parallel \mathrm{e}^{\chi_{0\mu}(z - z_1)}, \qquad z < z_1 \end{cases} \tag{25}$$

$$E^{\mathrm{TM}}_\parallel(k_\parallel, z) = \begin{cases} (1/\varepsilon_{M+1}) C_{M+1\,\mu} \chi_{M+1\,\mu} \mathrm{e}^{-\chi_{M+1\,\mu}(z - z_{M+1})}, \\ \qquad z > z_{M+1} \\ (\mathrm{i}/\varepsilon_j) q_{j\mu} [D_{j\mu} \mathrm{e}^{-\mathrm{i}q_{j\mu}(z - z_j - d_j/2)} \\ - C_{j\mu} \mathrm{e}^{\mathrm{i}q_{j\mu}(z - z_j - d_j/2)}], \\ \qquad z_j < z < z_j + d_j \\ (1/\varepsilon_0) D_{0\mu} \chi_{0\mu} e^{\chi_{0\mu}(z - z_1)}, \\ \qquad z < z_1 \end{cases} \tag{26}$$

where the electric field is obtained as $\mathbf{E}(\mathbf{r}) = \{[ic]/[\omega\varepsilon(\mathbf{r})]\}\nabla \times \mathbf{H}(\mathbf{r})$. As for TE-polarized modes, the $M+2$ coefficients in the above expressions are derived within the transfer-matrix theory together with the normalization integral (3).

3. Spontaneous emission rates

In this section the spontaneous transition rate of an excited atom embedded in a non-uniform dielectric medium (like the multilayer structure depicted in figure 1) is studied in a quantum-electrodynamical framework. We assume that the interaction between the excited two-level system and the e.m. field in the dielectric medium is not too strong, so that the transition between two states can be studied within the framework of perturbation theory. A detailed description of the canonical quantization of the e.m. field in a non-uniform medium [$\varepsilon = \varepsilon(\mathbf{r})$] is given in [23] and references therein, while here we recall the main results and provide the analytical expressions of the SE rates.

The starting point is an atom located at position z, which is initially in the excited state $|x\rangle$ (with energy $\hbar\omega_x$) and undergoes a spontaneous dipole transition to its ground state $|g\rangle$ (with energy $\hbar\omega_g$) by emitting a photon of energy $\hbar\omega_0 = \hbar\omega_x - \hbar\omega_g$. In the electric dipole approximation and near the atomic resonance ($\omega \approx \omega_0$), the atom–field interaction Hamiltonian for such a process is given by [33]

$$\hat{H}_{\gamma-A} \approx (\hat{\sigma}_+ \mathbf{d} + \hat{\sigma}_- \mathbf{d}^*) \cdot \hat{\mathbf{E}}(\mathbf{r}, t), \tag{27}$$

where $\hat{\sigma}_- = |g\rangle\langle x|$ ($\hat{\sigma}_+ = |x\rangle\langle g|$) is the atomic down- (up-) transition operator, $\mathbf{d} = \mathbf{d}_{xg} = \langle x|\hat{\mathbf{d}}|g\rangle = |\mathbf{d}|\hat{\varepsilon}_\mathrm{d}$ is the dipole matrix element, $\hat{\mathbf{d}} = e\hat{\mathbf{r}}$ being the atomic dipole operator of the atom located at $\mathbf{r}$ and $\hat{\mathbf{E}}(\mathbf{r})$ is the electric field operator:

$$\hat{\mathbf{E}}(\mathbf{r}, t) = \mathrm{i}\sum_{\mathbf{k},n}(2\pi\hbar\omega_{\mathbf{k}n})^{1/2} \times [\hat{a}_{\mathbf{k}n}\mathbf{E}_{\mathbf{k}n}(\mathbf{r})\mathrm{e}^{-\mathrm{i}\omega_{\mathbf{k}n}t} - \hat{a}^\dagger_{\mathbf{k}n}\mathbf{E}^*_{\mathbf{k}n}(\mathbf{r})\mathrm{e}^{\mathrm{i}\omega_{\mathbf{k}n}t}]. \tag{28}$$

In the expression given above $\hat{a}^\dagger_{\mathbf{k}n}$ ($\hat{a}_{\mathbf{k}n}$) are Bose creation (destruction) operators of field quanta with energies $\hbar\omega_{\mathbf{k}n}$ satisfying the usual commutation relations, n is a generic index labeling the eigenmode $\mathbf{E}_{\mathbf{k}n}$ and the following orthonormality condition holds [3, 25, 34]:

$$\int_V \varepsilon(\mathbf{r})\mathbf{E}^*_{\mathbf{k}n}(\mathbf{r}) \cdot \mathbf{E}_{\mathbf{k}'n'}(\mathbf{r})\mathrm{d}\mathbf{r} = \delta_{\mathbf{k},\mathbf{k}'}\delta_{n,n'}. \tag{29}$$

In the initial state $|i\rangle$ of the combined atom–radiation system there are no photons and the atom is in the upper (excited) level, i.e. $|i\rangle = |0\rangle \otimes |x\rangle$; in the final state $|f\rangle$ one photon is emitted in any mode of the e.m. field of frequency $\omega_{\mathbf{k}n}$ and the atom is in the lower (ground) level, $|f\rangle = |1_{\mathbf{k}n}\rangle \otimes |g\rangle$. By applying Fermi's Golden Rule (see, e.g., [35]) the spontaneous emission rate $\Gamma = \Gamma(\mathbf{r})$ of an atom located at position $\mathbf{r}$ is given by

$$\Gamma(\mathbf{r}) = \frac{2\pi}{\hbar^2}\sum_f \left|\langle f|\hat{H}_{\gamma-A}|i\rangle\right|^2 \delta(\omega_i - \omega_f), \tag{30}$$

where $\hbar\omega_i$ and $\hbar\omega_f$ are the energies of the initial and final state, respectively. By insertion of (28) in the above expression, and using the commutation rules for $\hat{a}_{\mathbf{k}n}$ and $\hat{a}^\dagger_{\mathbf{k}n}$, the spontaneous decay rate then is

$$\Gamma(\mathbf{r}) = \frac{4\pi^2|\mathbf{d}|^2}{\hbar}\sum_{\mathbf{k},n}|\mathbf{E}_{\mathbf{k}n}(\mathbf{r}) \cdot \hat{\varepsilon}_\mathrm{d}|^2\omega_{\mathbf{k}n}\delta(\omega_0 - \omega_{\mathbf{k}n}). \tag{31}$$

As discussed in section 2, an excited dipole embedded in a multilayer dielectric structure can decay either as a leaky or a guided eigenmode and, for both decay channels, two contributions to the total emission rate can be distinguished: (i) the emission rate $\Gamma_\parallel$ due to the decay of horizontal dipoles, i.e. in-plane oriented dipoles ($\hat{\varepsilon}_\mathrm{d} = \hat{x}$ or $\hat{y}$), which couple to both transverse electric (TE) and transverse magnetic (TM) polarized fields, and (ii) the rate $\Gamma_\perp$ due to the decay of vertical dipoles ($\hat{\varepsilon}_\mathrm{d} = \hat{z}$) which couple to TM-polarized modes only. Hence, for the realistic case of randomly oriented dipoles, the total emission rate averaged over the polarizations can be written as $\Gamma = (2/3)\Gamma_\parallel + (1/3)\Gamma_\perp$. Furthermore, since the dielectric function $\varepsilon(\mathbf{r}) = \varepsilon(z) = \varepsilon_j$ is homogeneous in each layer, the spontaneous emission rate will be expressed as a function of the z coordinate only. In the following part of this section we provide the exact expressions for the SE rates into leaky and guided modes.

3.1. Emission rates into leaky modes

As discussed in section 2.1, the leaky modes are specified by the propagation vector $(\mathbf{k}_\parallel, q)$ of the outgoing component. Hence, in (31), $\mathbf{k} = (\mathbf{k}_\parallel, q)$ and $n = (p, j)$ is a double index specifying the parameters of the final state, namely the field polarization p = TE, TM and the cladding layer j in which the emission occurs, $j = 0$ for emission in the lower cladding and $j = M + 1$ for emission in the upper cladding. The leaky mode dispersion $\omega = \omega_\gamma(\mathbf{k})$ is given by $\omega_\gamma = \frac{c}{\sqrt{\varepsilon_j}}(k_\parallel^2 + q^2)^{1/2}$ and for each propagation wavevector $\mathbf{k} = (\mathbf{k}_\parallel, q)$ the following relation holds:

$$k_\parallel^2 < k_j^2 = \varepsilon_j\frac{\omega_\gamma^2}{c^2}, \qquad j = 0, M+1, \tag{32}$$

i.e. the emission occurs within the light-cone in the $\{\omega, k_\parallel\}$ space and $\varepsilon_j = \varepsilon_0$ (ε_{M+1}) if the emission occurs in the lower (upper) cladding. By replacing $\omega_{\mathbf{k}n} = \omega_\gamma$ in (30), the emission rate into the leaky modes $\Gamma = \Gamma(z)$ can be written as

$$\Gamma(z) = \frac{4\pi^2|\mathbf{d}|^2\omega_0}{\hbar}J_\mathrm{leaky}(\omega_0, z), \tag{33}$$

where the TE- and TM-polarized fields $\mathbf{E}^\mathrm{TE}_{\mathbf{k}_\parallel}(\boldsymbol{\rho}, z)$ and $\mathbf{E}^\mathrm{TM}_{\mathbf{k}_\parallel}(\boldsymbol{\rho}, z)$ are given by (6) and (12), respectively, and $J_\mathrm{rad}(\omega_0, z)$ is the LDoS:

$$J_\mathrm{leaky}(\omega_0, z) = \frac{S}{(2\pi)^2}\sum_{p=\mathrm{TE,\ TM}}\sum_{j=0,\,M+1}\int|\mathbf{E}^p_{\mathbf{k}_\parallel}(\boldsymbol{\rho}, z) \cdot \hat{\varepsilon}_\mathrm{d}|^2 \times \rho_j(\mathbf{k}_\parallel, \omega)\,\mathrm{d}\mathbf{k}_\parallel. \tag{34}$$

In (34) $\rho_j(\mathbf{k}_\parallel, \omega)$ is the one-dimensional (1D) photon DoS at a fixed in-plane wavevector $\mathbf{k}_\parallel$, for leaky modes outgoing in the medium j:

$$\rho_j(\mathbf{k}_\parallel, \omega) = \frac{2\omega_0}{c^2}\sum_q\delta\left(\frac{\omega_0^2}{c^2} - \frac{\omega_\gamma^2}{c^2}\right) = \frac{L\sqrt{\varepsilon_j}\omega_0}{2\pi c}\frac{\Theta(\omega_0^2 - \frac{c^2k_\parallel^2}{\varepsilon_j})}{\sqrt{\omega_0^2 - \frac{c^2k_\parallel^2}{\varepsilon_j}}}, \tag{35}$$

where $L = V/S$ is the width of the normalization box in the z direction (which disappears in the final expression of the SE rate) and $\Theta[\Theta(x) = 1\,(=0)$ if $x > 0\,(x < 0)]$ is the Heaviside function. It is worth noticing at this point that, by using (34) with the basis of leaky modes discussed in section 2.1, the definition of the LDoS is unambiguous: for each outgoing mode ($j = 0$ or $M + 1$) the LDoS is defined by one mode component only and the difficulty related to the interference between components of different modes is thus avoided. Furthermore, due to the Heaviside function in (35), emission into partially leaky modes occurs only in the cladding with the higher refractive index, as it has to be. After the introduction of spherical coordinates in the $(\mathbf{k}_\parallel, q)$ space:

$$\mathbf{k}_\parallel = (k_j\sin\theta\cos\phi, k_j\sin\theta\sin\phi), \qquad \phi\,\epsilon[0, 2\pi], \quad \theta\,\epsilon[0, \pi/2], \tag{36}$$

the single contributions to the total emission rate $\Gamma = \Gamma(z)$ due to the decay of horizontal and vertical dipoles can be derived:

$$\Gamma_{\parallel}^{\mathrm{TE}}(z) = \frac{|\mathbf{d}|^2\omega_0^3}{2\hbar c^3} \sum_{j=0,\,M+1} \varepsilon_j^{3/2} \times \int_0^{\pi/2} |E^{\mathrm{TE}}(k_{\parallel} = k_j \sin\theta, z)|^2 \sin\theta \,\mathrm{d}\theta, \tag{37}$$

$$\Gamma_{\parallel}^{\mathrm{TM}}(z) = \frac{|\mathbf{d}|^2\omega_0}{2\hbar c[\varepsilon(z)]^2} \sum_{j=0,M+1} \varepsilon_j^{3/2} \times \int_0^{\pi/2} |E_{\parallel}^{\mathrm{TM}}(k_{\parallel} = k_j \sin\theta, z)|^2 \sin\theta \,\mathrm{d}\theta, \tag{38}$$

$$\Gamma_{\perp}^{\mathrm{TM}}(z) = \frac{|\mathbf{d}|^2\omega_0}{\hbar c[\varepsilon(z)]^2} \sum_{j=0,M+1} \varepsilon_j^{3/2} \times \int_0^{\pi/2} |E_{\perp}^{\mathrm{TM}}(k_{\parallel} = k_j \sin\theta, z)|^2 \sin\theta \,\mathrm{d}\theta, \tag{39}$$

where the field amplitudes E^{TE}, $E_{\parallel}^{\mathrm{TM}}$ and $E_{\perp}^{\mathrm{TM}}$ are given by (8), (15) and (14), respectively.

3.2. Emission rates into guided modes

Guided modes travel along the dielectric planes with propagation wavevector $\mathbf{k}_{\parallel}$, hence in (31) one takes $\mathbf{k} = \mathbf{k}_{\parallel}$, while $n = (p, \alpha)$, α is the guided mode index introduced in section 2.2. The spontaneous emission rate as a function of the 2D LDoS for guided modes J_{gui} is

$$\Gamma(z) = \frac{4\pi^2|\mathbf{d}|^2\omega_0}{\hbar} J_{\mathrm{gui}}(\omega_0, z), \tag{40}$$

where the fields $\mathbf{E}_{\mathbf{k}_{\parallel}}^{\mathrm{TE}}(\boldsymbol{\rho}, z)$ and $\mathbf{E}_{\mathbf{k}_{\parallel}}^{\mathrm{TM}}(\boldsymbol{\rho}, z)$ are given by (17) and (23), respectively, the sum extends over all the α guided modes and $J_{\mathrm{gui}}(\omega_0, z)$ is given by

$$J_{\mathrm{gui}}(\omega_0, z) = \frac{S}{(2\pi)^2} \sum_{p=\mathrm{TE},\,\mathrm{TM}} \sum_{\alpha} \int |\mathbf{E}_{\mathbf{k}_{\parallel}\alpha}^{p}(\boldsymbol{\rho}, z) \cdot \hat{\varepsilon}_{\mathrm{d}}|^2 \,\mathrm{d}\mathbf{k}_{\parallel}. \tag{41}$$

Integration over $\mathbf{k}_{\parallel}$ in (40) yields the following expressions for the single contributions $\Gamma_{\parallel}^{\mathrm{TE}}$, $\Gamma_{\parallel}^{\mathrm{TM}}$ and $\Gamma_{\perp}^{\mathrm{TM}}$:

$$\Gamma_{\parallel}^{\mathrm{TE}}(z) = \frac{|\mathbf{d}|^2\pi\omega_0^3}{\hbar c^2} \sum_{\alpha} |E^{\mathrm{TE}}(k_{\parallel} = k_0^{\alpha}, z)|^2 \frac{k_0^{\alpha}}{v_0^{\alpha}}, \tag{42}$$

$$\Gamma_{\parallel}^{\mathrm{TM}}(z) = \frac{|\mathbf{d}|^2\pi c^2}{\hbar\omega_0} \sum_{\alpha} |E_{\parallel}^{\mathrm{TM}}(k_{\parallel} = k_0^{\alpha}, z)|^2 \frac{k_0^{\alpha}}{v_0^{\alpha}}, \tag{43}$$

$$\Gamma_{\perp}^{\mathrm{TM}}(z) = \frac{|\mathbf{d}|^2 2\pi c^2}{\hbar\omega_0} \sum_{\alpha} |E_{\perp}^{\mathrm{TM}}(k_{\parallel} = k_0^{\alpha}, z)|^2 \frac{k_0^{\alpha}}{v_0^{\alpha}}, \tag{44}$$

where E^{TE}, $E_{\parallel}^{\mathrm{TM}}$ and $E_{\perp}^{\mathrm{TM}}$ are given by (19), (26) and (25), respectively. In the expressions given above, $k_0^{\alpha} = k_{\parallel}^{\alpha}(\omega = \omega_0)$ and $v_0^{\alpha} = (\mathrm{d}\omega_{\mathbf{k}_{\parallel}\alpha}/\mathrm{d}k_{\parallel})_{\omega_{\mathbf{k}_{\parallel}\alpha}=\omega_0}$ are the in-plane wavevector and the group velocity of the αth guided mode calculated at the dipole emission frequency ω_0, respectively. The wavevectors k_0^{α} as functions of the frequencies are the poles (which are real ones for guided modes) of the transmission amplitude $t = 1/T_{22}$ of the whole dielectric structure, T being the total transfer matrix for the multilayer structure considered. Notice that the total emission from planar dipoles is $\Gamma_{\parallel} = \Gamma_{\parallel}^{\mathrm{TE}} + \Gamma_{\parallel}^{\mathrm{TM}}$, while the emission from perpendicular dipoles is $\Gamma_{\perp} = \Gamma_{\perp}^{\mathrm{TM}}$. In an unpolarized experiment on randomly oriented dipoles, the average decay rate $\Gamma_{\mathrm{ave}} = (2/3)\Gamma_{\parallel} + (1/3)\Gamma_{\perp}$ is measured.

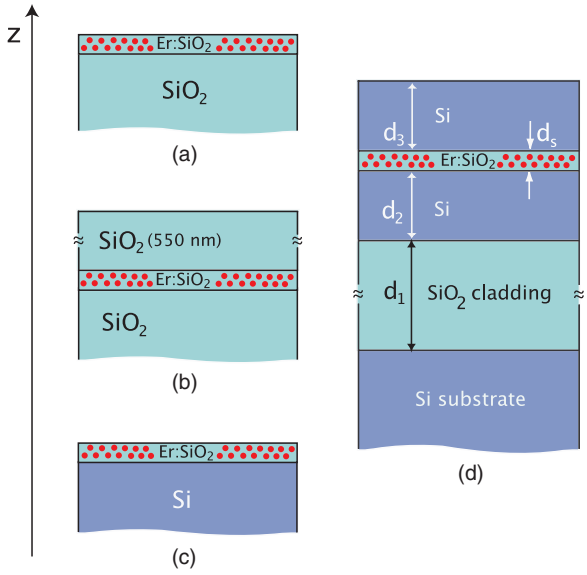

Figure 3. Schematic of the sample structures. Er-doped silicon oxide films $d_s = 20$ nm thick on silicon oxide (a), on silicon oxide and with a 550 nm thick SiO_2 layer on its top (b), on a crystalline silicon substrate (c) and embedded in the core of a slot waveguide (d), with $d_1 = 1.9$ μm and $d_2 = d_3 = 110$ nm.

4. Analysis of the 1.54 μm transition in Er^{3+}-doped SiO_2 layers

In this section we apply the model previously described to study in detail the photoluminescence (PL) decay rate of the $^4I_{13/2} \rightarrow {}^4I_{15/2}$ transition around 1.54 μm in Er^{3+}-doped SiO_2 planar slot layers acting as the active material in deposited polycrystalline silicon waveguides. As discussed in section 1 the lifetime of erbium ions can be drastically modified as a result of the confinement effects occurring in these structures. For a quantitative evaluation of this effect, we have analyzed the decay rates of Er-doped SiO_2 layers of the same thickness in three other configurations, namely after deposition on SiO_2 and Si substrates and embedded in an SiO_2 bulk. Furthermore, by combining the radiative SE rates obtained from the quantum-electrodynamical formalism with time-resolved PL measurements, we are also able to evaluate the non-radiative decay rates and the radiative efficiency.

4.1. Structures and measurements

A schematic of the cross section of the four investigated structures is depicted in figure 3. Er-doped silicon oxide thin films, about $d_s = 20$ nm thick, have been deposited by reactive co-sputtering from SiO_2 and Er_2O_3 targets. The depositions have been realized in a reactive atmosphere (90% Ar and 10% O_2) by keeping the substrate heated at 300 °C. The films

are located on a 1.9 μm thick thermal SiO_2 layer (structure (a)), within bulk-like SiO_2 (structure (b)) by depositing a 550 nm thick SiO_2 layer on top of structure (a), on a (100) crystalline silicon (c-Si) substrate (structure (c)) and within the silicon core of a slot waveguide (structure (d)). The slot waveguide consists of the sequence of Si(110 nm)/Er:SiO_2 (20 nm)/Si(110 nm) layers deposited on top of a 1.9 μm thick silicon dioxide layer thermally grown on a silicon substrate. The silicon layers have been realized by sputtering an Si cathode in a pure Ar atmosphere without heating the substrate. Structures (a) and (b) also lie on a Si substrate (not shown in figures 3(a) and (b) for the sake of clarity). After the deposition all the films have been annealed at 900 °C for 1 h in a nitrogen atmosphere. The Er content, measured by Rutherford backscattering spectrometry, is constant within the thin SiO_2 layers, with a concentration of 7.6×10^{19} cm^{-3} for all the samples.

Time-resolved PL at room temperature was performed by pumping with the 488 nm line of an Ar^+ laser, the laser beam being chopped through an acousto-optic modulator at a frequency of 11 Hz. The laser was focused on the sample's surface at an angle of 60° and then the emitted light was collected in the normal direction for all four structures here examined and depicted in figure 3. The modulated luminescence signal, unpolarized, was first spectrally resolved by a single grating monochromator set at 1535 nm with a resolution of 6 nm, detected with a Hamamatsu infrared-extended photomultiplier tube, and then analyzed with a photon counting multichannel scaler with an overall time resolution of 30 ns. It is worth noticing that the PL decay rate is independent of the detection direction. This can be easily understood in terms of the expression giving the number of dipoles $n(t)$ decaying at a certain time t after the initial excitation, i.e. $n(t) = n_0 e^{-\Gamma_{tot} t}$. The measured decay rate $\tau_{tot} = 1/\Gamma_{tot}$ is just the time constant of such a process and is, of course, independent of the decay direction of the excited dipoles. In the case of structure (d) (slot waveguide) supporting guided modes, the total SE rate is the sum of the contributions due to emission into guided and leaky modes, i.e. $\Gamma_{tot} = \Gamma_{gui} + \Gamma_{leaky}$, but again, detecting the PL signal either from the top or from the waveguide edge, yields the same result in terms of decay rate $\tau_{tot} = 1/\Gamma_{tot}$. The choice of surface emission geometry for time-resolved PL measurements is therefore appropriate in order to compare and reveal the trends when going through structures (a)–(d), as we now discuss.

The PL decay curves at 1.5 μm give a direct measurement of the decay rate of the first excited multiplet ($^4I_{13/2}$) of Er^{3+} and are shown in figure 4: all of them are characterized by a single exponential behavior, and the lifetimes were determined to be $\tau^a = 12.98 \pm 0.03$ ms, $\tau^b = 10.37 \pm 0.03$ ms, $\tau^c = 4.02 \pm 0.03$ ms and $\tau^d = 1.336 \pm 0.008$ ms for Er-doped SiO_2 deposited on SiO_2, embedded in SiO_2, deposited on c-Si and embedded within the slot waveguide, respectively. With respect to Γ^a the measured decay rate $\Gamma = 1/\tau$ is thus enhanced by a factor $\Gamma^b/\Gamma^a = 1.25$, $\Gamma^c/\Gamma^a = 3.23$ and $\Gamma^d/\Gamma^a = 9.71$. The lifetime τ^b of the Er-doped SiO_2 film embedded in SiO_2 (structure (b) in figure 1), i.e. the *bulk lifetime*, is similar to the value of 9.5 ms reported in [36] for films synthesized by e-beam deposition and of about 15 ms for thermally grown silicon oxide layer [20, 37].

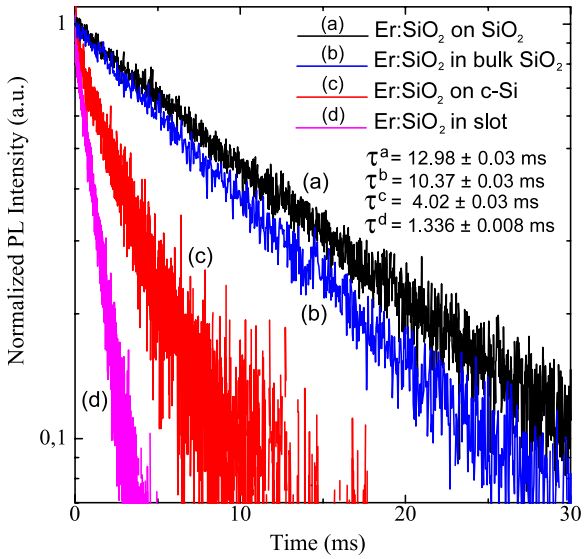

Figure 4. Erbium PL intensity decay curves (in log scale) for the structures depicted in figure 3. The intensities are normalized to their corresponding maxima.

The decrease in the observed lifetime τ^c relative to τ^a is consistent with the effect of the dielectric mismatch at the Si/SiO_2 interface which results in a concentration of the e.m. field in a narrow spatial region across it and thus to an enhancement of the radiative spontaneous emission rate. However, to properly address the issue of the modified lifetime of Er^{3+}, both the radiative (Γ_{rad}) and the non-radiative (Γ_{nrad}) recombination rates need to be estimated, since the measured decay rate $\Gamma = 1/\tau = \Gamma_{rad} + \Gamma_{nrad}$ sums up both contributions.

4.2. Radiative and non-radiative decay rates

In a generic dielectric multilayer structure, the total radiative decay rate Γ_{rad} results from the emission into leaky and guided modes (if any), $\Gamma_{rad} = \Gamma_{rad}^{leaky} + \Gamma_{rad}^{gui}$, the latter being supported by the slot waveguide only (structure (c)) among the structures here considered and shown in figure 3.

The radiative SE rates $\Gamma_{rad} = 1/\tau_{rad}$ can be easily calculated within the quantum-electrodynamical formalism described in section 3 through (37)–(39) and (42)–(44) with the same parameters (thicknesses and refractive indices) of the four considered structures and for the realistic case of a randomly oriented Er^{3+} emitter in an SiO_2 layer. It is worth noticing at this point that, since the Er^{3+} ions are always embedded in the same SiO_2 dielectric material, local field effects (see, e.g., [38] and references therein) are not relevant and thus have not been involved in the present theoretical analysis. The radiative decay rates are found to be in the following ratios: $\Gamma_{rad}^b/\Gamma_{rad}^a = 1.4$, $\Gamma_{rad}^c/\Gamma_{rad}^a = 2.4$ and $\Gamma_{rad}^d/\Gamma_{rad}^a = 8.9$. As expected, a significant increase of the radiative decay rate occurs in the slot waveguide ($\Gamma_{rad}^d/\Gamma_{rad}^a = 8.9$): in this case the high-index-contrast which develops at

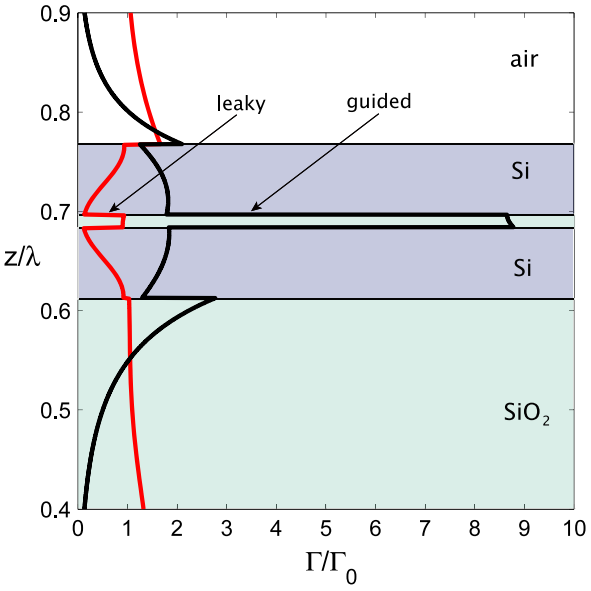

Figure 5. The normalized (with respect to the vacuum emission rate Γ_0) radiative spontaneous emissions rates $\Gamma_{\rm rad} = (2/3)\Gamma_{\parallel} + (1/3)\Gamma_{\perp}$ for a slot waveguide calculated as a function of the dipole position z/λ (λ being the emission wavelength). The black and red lines refer to the normalized emission rates into guided and leaky modes, respectively. The refractive index of Si is taken to be $n = 3.48$ and that of SiO_2 (both undoped and Er-doped) is $n = 1.45$.

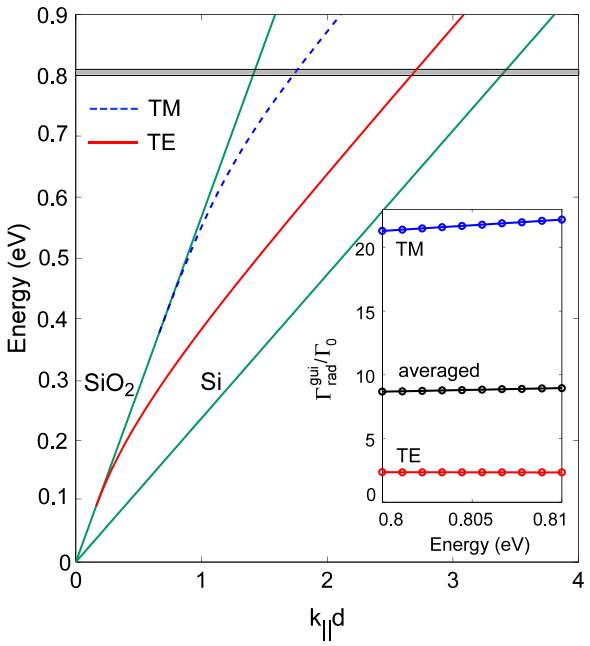

Figure 6. The dispersion of guided modes supported by the slot waveguide with a core of thickness $d = d_2 + d_S + d_3$ (see structure (d) in figure 3). Blue-dashed and red-continuous lines refer to TM- and TE-polarized modes, respectively. The shadowed region around 0.8 eV shows the main erbium emission spectrum (0.8–0.81) eV. The light lines of Si and SiO_2 are also shown. Inset: the normalized SE rates into guided modes as a function of the erbium emission energy; the average emission $\Gamma_{\rm ave} = (2/3)(\Gamma_{\parallel}^{\rm TE} + \Gamma_{\parallel}^{\rm TM}) + (1/3)\Gamma_{\perp}^{\rm TM}$ and the emission rates $\Gamma^{\rm TE} = \Gamma_{\parallel}^{\rm TE}$ and $\Gamma^{\rm TM} = \Gamma_{\parallel}^{\rm TM} + \Gamma_{\perp}^{\rm TM}$ into TE and TM modes, respectively, are shown.

the Er:SiO_2/Si interfaces of the slot leads to a strong field confinement for TM modes, due to the discontinuity of the z component of the electric field, and thus to an enhanced radiative emission as a result of the increase of the local density of optical states. Such an enhancement is mainly due to the emission into guided modes as is clear from figure 5 which shows the separate emission rates into leaky and guided modes (see the black and red lines) calculated as a function of the Er^{3+} position (z/λ) in the slot waveguide (structure (d) in figure 3), with a calculated ratio $\Gamma_{\rm rad}^{\rm gui}/\Gamma_{\rm rad}^{\rm leaky} \approx 9$ when the erbium ions are placed in the slot region. These results are thus consistent with light confinement effects which have been recently observed in similar active slot waveguides [24] where an enhancement of TM- over TE-polarized guided mode emission was demonstrated. In figure 6 we show the calculated dispersion of guided modes supported by the slot waveguide here considered (structure (d) in figure 3) and the related SE rate (see the inset) as a function of the erbium energy: it can be seen that the emission properties of erbium are basically independent of the wavelength within its main emission spectrum (depicted in figure 6 with the shadowed region corresponding to the energy range (0.80–0.81) eV). It can be interesting to establish the maximum enhancement of radiative rate that can be obtained in these slot waveguides: as the slot width goes to zero, the ratio $\Gamma_{\rm rad}^{\rm d}/\Gamma_{\rm rad}^{\rm b}$ grows towards the limiting value $(\varepsilon_{\rm Si}/\varepsilon_{\rm SiO_2})^2 \simeq 33.25$ ($\varepsilon_{\rm Si}$ and $\varepsilon_{\rm SiO_2}$ being the dielectric constants of Si and SiO_2, respectively) for TM polarization and $\simeq 12$ when averaged over polarizations. Thus the ratio $\Gamma_{\rm rad}^{\rm d}/\Gamma_{\rm rad}^{\rm a}$ averaged over polarizations tends to $\simeq$16. For the present case of a 20 nm thick slot layer, the theoretical ratio is $\Gamma_{\rm rad}^{\rm d}/\Gamma_{\rm rad}^{\rm a} = 8.9$, but a thinner slot layer would not necessarily yield better results for radiative lifetime reduction, both because the emitter's luminescence would be even weaker and non-radiative processes due to interaction with defects at slot interfaces would be enhanced.

The radiative and non-radiative contributions to the total emission rates can be evaluated by combining the measured PL decay rates and theoretical ratios $\beta_{\rm b}^{\rm a,c,d}$ defined as

$$\beta_{\rm b}^{\rm a,c,d} = \Gamma_{\rm rad}^{\rm a,\ c\ ,d}/\Gamma_{\rm rad}^{\rm b}. \tag{45}$$

The procedure is the following. The emission rates $\Gamma_{\rm rad}^{\rm b}$ and $\Gamma_{\rm nrad}^{\rm b}$ for Er-doped SiO_2 in bulk SiO_2 (structure (b) in figure 1) have been first determined. This can be done by solving the coupled equations for the variables $\Gamma_{\rm rad}^{\rm b}$ and $\Gamma_{\rm nrad}^{\rm b} = \Gamma_{\rm nrad}^{\rm a}$ given by

$$\begin{aligned} \Gamma^{\rm a} &= \Gamma_{\rm rad}^{\rm a} + \Gamma_{\rm nrad}^{\rm a} = \beta_{\rm b}^{\rm a}\Gamma_{\rm rad}^{\rm b} + \Gamma_{\rm nrad}^{\rm a}, \\ \Gamma^{\rm b} &= \Gamma_{\rm rad}^{\rm b} + \Gamma_{\rm nrad}^{\rm b} \approx \Gamma_{\rm rad}^{\rm b} + \Gamma_{\rm nrad}^{\rm a}, \end{aligned} \tag{46}$$

where $\Gamma^{\rm a,b} = 1/\tau^{\rm a,b}$ are the SE rates obtained from the PL measurements, $\beta_{\rm b}^{\rm a}$ is given by (45), and we have assumed $\Gamma_{\rm nrad}^{\rm a} \approx \Gamma_{\rm nrad}^{\rm b}$, i.e. the non-radiative processes in structures (a) and (b) being approximately the same. This assumption is fully reasonable, since the non-radiative recombination processes in SiO_2 are due to short-range Förster energy transfer between the Er^{3+} transition and the resonant hydroxyl groups [20] and thus have the same efficiency in both structures (a) and (b).

By solving (46), the radiative efficiency for Er:SiO_2 in SiO_2 bulk has been determined to be $q = \Gamma^{b}_{rad}/(\Gamma^{b}_{rad} + \Gamma^{b}_{nrad}) = 0.74$, a value very close to that given in [37] for similar structures. Once Γ^{b}_{rad} has been determined, the radiative emission rates $\Gamma^{a,c,d}_{rad}$ for structures (a), (c) and (d) are found as $\Gamma^{a,c,d}_{rad} = \beta^{a,c,d}_{b}\Gamma^{b}_{rad}$ by using the ratios given in (45). Then, the non-radiative rates $\Gamma^{a,c,d}_{nrad}$ can be obtained as the differences between the experimental decay rates $\Gamma^{a,c,d} = 1/\tau^{a,c,d}$ and the theoretical radiative ones, i.e. $\Gamma^{a,c,d}_{nrad} = \Gamma^{a,c,d} - \Gamma^{a,c,d}_{rad}$.

The measured decay rates and the calculated radiative and non-radiative contributions are all shown in figure 7. First, it can be clearly seen that, as the average refractive index at the Er-doped SiO_2 layer increases (see the structures from left to right), so does the radiative decay rate of the Er^{3+} transition and a strong lifetime reduction does occur when the layer is embedded within the slot waveguide. Furthermore, the non-radiative decay rate increases as well in the Er-doped SiO_2 on c-Si and in the slot waveguide structures ((c) and (d) in figure 3) as a result of the interaction of the Er^{3+} transition with surface defect states at the SiO_2/Si interfaces and to Auger quenching with free and bound carriers in silicon. This effect has been thoroughly studied in the past, see, e.g., [39–41]. Notice that the non-radiative decay rate in structures (c) and (d) can be distributed quite inhomogeneously within the Er-containing slab, so that the effective non-radiative decay rate is an average over the active layer thickness. In spite of these complications, the radiative quantum efficiency is estimated to be about 62% in structure (d), this latter value being only slightly smaller than in bulk SiO_2. Hence, the radiative recombination is still the dominant process in the slot waveguide.

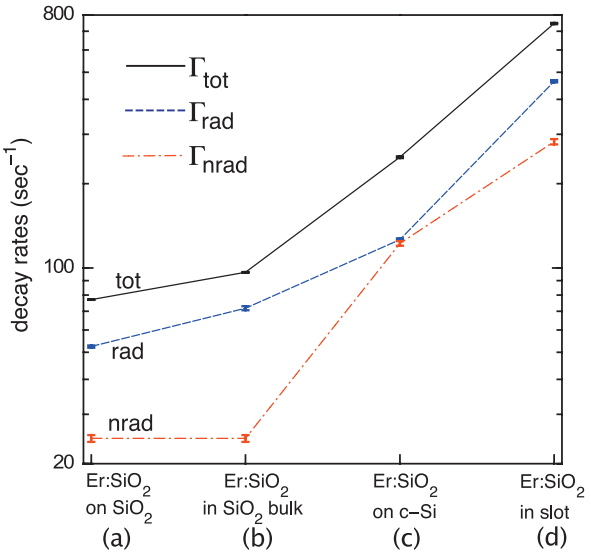

Figure 7. Erbium photoluminescence decay rates (in log scale). Black continuous line: the measured decay rates $\Gamma_{tot} = \Gamma_{rad} + \Gamma_{nrad}$. Blue dashed and red dash-dotted lines: the radiative and non-radiative rates, respectively, evaluated using the measured PL decay rates and the theoretical ratios $\beta^{a,c,d}_{b} = \Gamma^{a,c,d}_{rad}/\Gamma^{b}_{rad}$. The error bars for the experimental decay rates (black continuous line) are those associated with the lifetimes derived from the PL decay curves (see figure 2). The uncertainties in the radiative and non-radiative rates have been obtained by applying error propagation.

5. Conclusions

We have described a quantum-electrodynamical formalism which is particularly suitable to study the spontaneous emission in generic lossless and non-dispersive multilayer dielectric structures. The analytical expressions for the local density of states and spontaneous emission rate into leaky and guided modes have been derived as a function of the excited dipole position in the considered structure. By describing the leaky modes with a basis specified by a single outgoing radiative component, the total emission rate as well as the emission in the upper/lower claddings or, more generally, the SE patterns, can be calculated in a straightforward way, avoiding all the difficulties related to the treatment of interference terms which arise when the standard (Carniglia and Mandel) basis is used.

This model has been applied to study in detail the decay rate of the 1.5 μm transition of Er^{3+}-doped SiO_2 layers embedded in Si-based waveguides. We have shown that, when a tiny layer of doped SiO_2 is embedded within the core of a silicon-based optical waveguide (slot waveguide configuration), a strong reduction of the radiative lifetime of Er^{3+} occurs. This result can be regarded as the analog of the Purcell effect in an optical cavity and can be a major step towards achieving gain and stimulated emission in Er-doped silicon-based slot waveguides. Moreover, by combining the theoretical results and time-resolved PL measurements, we have also estimated the non-radiative contributions to the total decay rate, which has been found to be strongly increased when the Er:SiO_2 layer is deposited on a silicon substrate and embedded in the slot waveguide. This is probably due to recombination with surface defects at the SiO_2/silicon interface and to Auger quenching. However, since the estimated radiative efficiency is about 62% in the slot waveguide, radiative recombination is still the dominant decay mechanism thanks to the increase of radiative decay rate in the slot that more than compensates the increase of non-radiative decay rate.

References

[1] Purcell E M 1946 Spontaneous emission probabilities at radio frequencies *Phys. Rev.* **69** 674
[2] van Tiggelen B A and Kogan E 1994 Analogies between light and electrons: density of states and Friedels identity *Phys. Rev.* A **49** 708–13
[3] Glauber R J and Lewenstein M 1991 Quantum optics of dielectric media *Phys. Rev.* A **43** 467–91
[4] Drehhage K H 1974 *Progress in Optics* (Amsterdam: North-Holland)
[5] Wylie J M and Sipe J E 1984 Quantum electrodynamics near an interface *Phys. Rev.* A **30** 1185–93
Wylie J M and Sipe J E 1985 Quantum electrodynamics near an interface. II *Phys. Rev.* A **32** 2030–43
[6] Khosravi H and Loudon R 1991 Vacuum field fluctuations and spontaneous emission in the vicinity of a dielectric surface *Proc. R. Soc.* A **433** 337–52
[7] Janowicz M and Żakowicz W 1994 Quantum radiation of a harmonic oscillator near the planar dielectric-vacuum interface *Phys. Rev.* A **50** 4350–64

[8] Snoeks E, Lagendijk A and Polman A 1995 Measuring and modifying the spontaneous emission rate of erbium near an interface *Phys. Rev. Lett.* **74** 2459–62
[9] Barnes W L 1998 Fluorescence near interfaces: the role of photonic mode density *J. Mod. Opt.* **45** 661–99
[10] Inoue T and Hori H 2001 Quantization of evanescent electromagnetic waves based on detector modes *Phys. Rev.* A **63** 063805
[11] Wang F H, Jin Y P, Gu B Y, Zhou Y S and Wang X H 2005 Application of closed-orbit theory to the spontaneous emission of atoms near a single dielectric interface *Phys. Rev.* A **71** 044901
[12] Björk J, Machida S, Yamamoto Y and Igeta K 1991 Modification of spontaneous emission rate in planar dielectric microcavity structures *Phys. Rev.* A **44** 669–81
[13] Rigneault H and Monneret S 1996 Modal analysis of spontaneous emission in a planar microcavity *Phys. Rev.* A **54** 2356–68
[14] Rigneault H, Robert S, Begon C, Jacquier B and Moretti P 1997 Radiative and guided wave emission of Er^{3+} s atoms located in planar multidielectric structures *Phys. Rev.* A **55** 1497–502
[15] Benisty H, Stanley R and Mayer M 1998 Method of source terms for dipole emission modification in modes of arbitrary planar structures *J. Opt. Soc. Am.* A **15** 1192–201
[16] Lee K K, Lim D R, Kimerling L C, Shin J and Cerrina F 2001 Fabrication of ultralow-loss Si/ SiO_2 waveguides by roughness reduction *Opt. Lett.* **26** 1888–90
[17] Vlasov Y A and McNab S J 2004 Losses in single-mode silicon-on-insulator strip waveguides and bends *Opt. Express* **12** 1622–31
[18] Almeida V R, Barrios C A, Panepucci R R and Lipson M 2004 All-optical control of light on a silicon chip *Nature* **431** 1081–4
[19] Kenyon A J 2005 Erbium in silicon *Semicond. Sci. Technol.* **20** R65–84
[20] Polman A 1997 Erbium implanted thin film photonic materials *J. Appl. Phys.* **82** 1–39
[21] Almeida V R, Xu Q, Barrios C A and Lipson M 2004 Guiding and confining light in void nanostructure *Opt. Lett.* **29** 1209–11
[22] Xu Q, Almeida V R, Panepucci R R and Lipson M 2004 Experimental demonstration of guiding and confining light in nanometer-size low-refractive-index material *Opt. Lett.* **29** 1626–8
[23] Creatore C and Andreani L C 2008 Quantum theory of spontaneous emission in multilayer dielectric structures *Phys. Rev.* A **78** 063825
[24] Galli M *et al* 2006 Direct evidence of light confinement and emission enhancement in active silicon-on-insulator slot waveguides *Appl. Phys. Lett.* **89** 241114
[25] Carniglia C K and Mandel L 1971 Quantization of evanescent electromagnetic waves *Phys. Rev.* D **3** 280–96
[26] Khosravi H and Loudon R 1992 Vacuum field fluctuations and spontaneous emission in a dielectric slab *Proc. R. Soc.* A **436** 373–89
[27] Urbach H P and Rikken G L J A 1998 Spontaneous emission from a dielectric slab *Phys. Rev.* A **57** 3913–30
[28] Hooijer C, Li G X, Allaart K and Lenstra D 2001 Spontaneous emission in multilayer semiconductor structures *IEEE J. Quantum Electron.* **37** 1161–70
[29] Żakowicz W 1995 Interference and angular distribution of transition radiation *Phys. Rev.* A **52** 882–3
[30] Glauber R J and Lewenstein M 1995 Reply to 'interference and angular distribution of transition radiation' *Phys. Rev.* A **52** 884
[31] Yariv A 1989 *Quantum Electronics* (New York: Wiley)
[32] Andreani L C and Gerace D 2006 Photonic-crystal slabs with a triangular lattice of triangular holes investigated using a guided-mode expansion method *Phys. Rev.* B **73** 235114
[33] Sakurai J J 1982 *Advanced Quantum Mechanics* (Reading, MA: Addison-Wesley)
[34] Bhat N A R and Sipe J E 2006 Hamiltonian treatment of the electromagnetic field in dispersive and absorptive structured media *Phys. Rev.* A **73** 063808
[35] Loudon R 1983 *The Quantum Theory of Light* (Oxford: Clarendon)
[36] Vredenberg A M, Hunt N E J, Schubert E F, Jacobson D C, Poate J M and Zydzik G J 1993 Controlled atomic spontaneous emission from Er^{3+} in a transparent Si/SiO_2 microcavity *Phys. Rev. Lett.* **71** 517–20
[37] Bao J, Yu N, Capasso F, Mates T, Troccoli M and Belyanin A 2007 Controlled modification of erbium lifetime in silicon dioxide with metallic overlayers *Appl. Phys. Lett.* **91** 131103
[38] Zampedri L, Mattarelli M, Montagna M and Gonçalves R R 2007 Evaluation of local eld effect on the $^4I_{13/2}$ lifetimes in Er-doped silica-hafnia planar waveguides *Phys. Rev.* B **75** 073105
[39] Langer J M and Van Hong L 1984 Gd^{3+} and Tb^{3+} luminescence quenching by the Auger effect in CdF_2 crystals *J. Phys. C: Solid State Phys.* **17** L923–7
[40] Suchocki A and Langer J M 1989 Auger effect in the Mn^{2+} luminescence of CdF_2:(Mn, Y) crystals *Phys. Rev.* B **39** 7905–15
[41] Priolo F, Franzò G, Coffa S and Carnera A 1998 Excitation and nonradiative deexcitation processes of Er^{3+} in crystalline Si *Phys. Rev.* B **57** 4443–55